39th IAHR WORLD CONGRESS GRANADA, SPAIN 2022 From Snow to Sea 19-24 June 2022

Proceedings of the 39th IAHR World Congress
19–24 June 2022, Granada, Spain
doi://10.3850/IAHR-39WC2521716X2022115

Turbulence Driven Secondary Currents in a Partially Filled Pipe

Yan Liu[(1)] and Thorsten Stoesser[(2)]

[(1,2)] Department of Civil, Environmental and Geomatic Engineering, University College London, London, UK
e-mail (ucesy10@ucl.ac.uk)
e-mail (t.stoesser@ucl.ac.uk)

Abstract

This paper provides details of the physical mechanisms that lead to the so-called 'velocity dip' in partially-filled pipe flows and reveals the interactions between the water surface and the turbulent flow underneath it. Therefore, large eddy simulations of a semi-filled pipe are performed. It is observed that a single pair of symmetric vortices about the vertical pipe bisector forms as a result of the wall-water surface junction turbulence anisotropy. At this wall-water surface junction, imbalance of the production, dissipation and transport of turbulent kinetic energy (TKE) leads to non-zero TKE convection, which drives the secondary flow. The distribution of the instantaneous velocity reveals the signatures of wall-bounded turbulent flows near the pipe wall such as large-scale motions and associated hairpin vortices which are convected towards the water surface. Free surface fluctuations are observed which are caused by these hairpin vortices reaching the water surface.

Keywords: Partially filled pipe flow; Large eddy simulations; Turbulent flow; Hairpin vortex

1. INTRODUCTION

Partially-filled pipe flow has received far less attention than its fully-filled counterpart, though this type of flow has many important engineering applications such as wastewater flow in sewers. One significant difference is the presence of secondary currents in partially filled pipe flow, due to non-circular fluid cross section area (Prandtl 1926; Bradshaw 1987) and variations in surface roughness/shear between the pipe walls and the gas-liquid interface (Vollestad et al. 2020). Secondary currents are found to influence the primary mean-velocity field as well as the distribution of Reynolds stresses (Ng et al. 2018), subsequently leading to changes of the streamwise pressure gradient and the friction factor in pipes. Therefore, it is of great scientific and practical interests to understand in detail turbulence driven secondary currents in partially-filled pipe.

In 1926, Prandtl (1926) was the first to observe turbulence driven secondary currents and he classified them secondary currents of the second kind. A good amount of research has revealed the origin of turbulence driven secondary currents (Hinze, 1967; Nezu, 2005; Uhlmann et al., 2007; Pirozzoli et al., 2018). For example, Hinze (1967) showed that the imbalance between the external energy supply to the mean flow and the energy dissipation in various regions of the flow is the origin of secondary currents based on the turbulent kinetic energy equation. Nezu (2005) explained through the streamwise vorticity equation that turbulence driven secondary currents are generated by turbulence inhomogeneity and anisotropy. These theoretical findings have encouraged more detailed studies on the inter-relation between secondary currents and turbulence. For example, Pinelli et al. (2010) performed direct numerical simulations of smooth-wall turbulent flow in a straight square duct with a particular focus on the role of coherent structures in the generation and characterization of near-corner secondary cells. They found that the buffer layer structures determine the distribution of mean streamwise vorticity, while the shape of the cells is influenced by larger-scale motions. For open channel flow, Albayrak (2008) carried out extensive experiments in a large, straight, gravel bed flume, and their results showed that the time-averaged secondary flow cells represent large instantaneous helical structures. Based on the eddy cascade concept, Nikora and Roy (2012) proposed that secondary flows in straight channels receive their energy from turbulence, suggesting the existence of an inverse energy cascade (i.e., flux of energy from smaller scales to larger scales to the mean flow) regions of the flow.

Despite significant progress in the mechanism of turbulence driven secondary currents in open channel flows and duct flows, the effects of turbulence driven secondary currents in partially filled pipe flow on flow, turbulence and bulk flow resistance is poorly understood. Previous experimental work on smooth-walled circular cross-section pipe flow running partially full focused on the effects on the bulk frictional losses. Swaffield and Bridge (1983) reviewed frictional losses in partially filled conduits and Enfinger and Kimbrough

(2004), Enfinger and Schutzbach (2005) assessed the value of Manning's coefficient for circular open channels. And due to sparse measurements of velocity fields in partially filled pipe flow, most of the studies focused only on the bulk flow behavior for example: Knight and Sterling (2000) and Sterling and Knight (2000) report the mean streamwise velocity distribution measured using a Pitot-static tube for a smooth circular pipe running partially full while Ead et al. (2000) reported on the mean streamwise velocity profiles in the centreline of a corrugated culvert; Clark and Kehler (2011) reported on the mean velocity distribution and turbulent stress profiles in a corrugated culvert using acoustic Doppler velocimetry (ADV). The recently developed technique of stereoscopic particle image velocimetry (S-PIV) is considered a powerful tool for understanding the inter-relation between secondary currents and turbulence. Ng et al. (2018) applied S-PIV to measure the 3D velocity field in partially filled pipes with different water depths. Their results show that the large-scale coherent motions present in fully-filled pipe flow persist in partially filled pipes but are compressed and distorted by the presence of the free surface and the mean secondary motion. Birvalski et al. (2014) investigated experimentally partially filled pipe flows with different air/liquid velocity ratios. Their results revealed that secondary currents in the liquid phase would have opposite directions in the pipe center (i.e. upward toward the interface or downward away from the interface) for different air/liquid velocity ratios.

Besides those experimental efforts, numerical simulations have also been employed to study partially-filled pipe flows (Berthelsen and Ytrehus 2007; Duan et al. 2014; Fullard and Wake 2015). These simulations did not reveal the mechanism of turbulence driven currents. For example, the numerical simulations by Fullard and Wake (2015) and Duan et al. (2014) focused on laminar flows. Whereas Berthelsen and Ytrehus (2007) studied stratified two-phase flows by using a Reynolds- averaged Navier Stokes (RANS) model, which is unable to resolve the turbulence anisotropy near the water surface and hence their simulations did not resolve the resulting turbulence driven secondary currents.

In this study, large-eddy simulations are carried out to complement and extend the work by Ng et al. (2018). The objective of the study reported here is to investigate the effect of turbulence driven secondary currents on the flow and turbulence characteristics in partially-filled pipes.

2. NUMERICAL FRAMEWORK

In this study the method of large-eddy simulation (LES), using the code Hydro3D an eddy-resolving numerical method, is used for the turbulent flow. Hydro3D has been validated and applied to several flows of similar complexity to the one reported here (Liu et al, 2017; Fang et al, 2017; Liu et al, 2019a; Liu et al, 2019b). The code is based on finite differences on a staggered Cartesian grid and solves the filtered Navier-Stokes equations for incompressible, unsteady and viscous flow:

$$\frac{\partial u_i}{\partial x_i} = 0 \qquad [1]$$

$$\frac{\partial u_i}{\partial t} + \frac{\partial u_i u_j}{\partial x_j} = -\frac{1}{\rho}\frac{\partial p}{\partial x_i} + \frac{\partial \left(2\nu S_{ij}\right)}{\partial x_j} - \frac{\partial \tau_{ij}}{\partial x_j} \qquad [2]$$

where u_i or u_j is the resolved velocity vector (i or j = 1, 2, and 3 represent x-, y- and z-axis directions, respectively); and similarly x_i, x_j represent the spatial vectors in the three directions; ρ is water density; p is the resolved pressure divided by the density; υ = kinematic viscosity; and S_{ij} is the strain strain-rate tensor. The sub-grid scale (SGS) stress is defined as $\tau_{ij} = -2\nu_t S_{ij}$, and in this study the wall-adapting local eddy viscosity (WALE) proposed by Nicoud and Ducros (1999) is used to compute the SGS stress.

The convection and diffusion terms in the Navier-Stokes equations are approximated by 4th-order accurate central differences. An explicit 3-step Runge-Kutta scheme is used to integrate the equations in time, providing 2nd-order accuracy. A fractional step method is employed, that is within the time step, convection and diffusion terms are solved explicitly first in a predictor step which is then followed by a corrector step during which the pressure and divergence-free-velocity fields are obtained through a Poisson equation. The latter is solved iteratively through a multi-grid procedure. The location of the water surface is calculated in every time step using the level-set method (Osher and Sethian 1988), in which the flow domain consists of an air and a water phase and an interface in between the two, the so-called level set. More details of the code are reported in Mcsherry et al. (2018).

Figure 1 presents a cross-section of the flow in a partially-filled pipe with the pipe radius R, flow depth in the centre h and the water surface width B. The computational setup of the LES is very similar to the laboratory experiment conducted by Ng et al. (2018), the data of which are used to validate the simulations. The water depth is h/D=52% and the bulk velocity is U_b = 0.289, resulting in bulk Reynolds numbers of Re_b=30010 and Froude numbers of Fr=0.43 as given in table 1. The bulk Reynolds number Re_b is defined as $Re_b = 4R_hU_b$, where R_h is the hydraulic radius being the ratio of flow cross-sectional area and wetted perimeter. The length of the pipe is Lx = 22R and is considered sufficiently long enough to allow the

development of very-large-scale motion (VLSM) as VLSM in fully-filled pipe flow was observed to have a streamwise length scale of $\lambda_x = 8R \sim 16R$ (Kim and Adrian 1999). The spanwise and vertical dimension of the computational domain is set as Ly = Lz = 1.08D, i.e. slightly larger than the diameter of the pipe, because extra grid points are required for representing the pipe walls using the immersed boundary (IB) method proposed by Uhlmann (2005). The IB method enforces the no-slip condition at smooth walls and requires a sufficiently fine grid. Periodic boundary conditions are applied in the streamwise direction. The location of the water surface is computed in every time step using the level-set method which does not require explicit specification of a boundary condition.

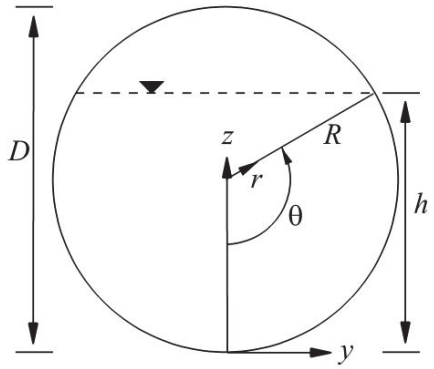

Figure 1. Cross-section of pipe showing definitions of depth and free surface width.

The simulations are carried out on different grids and only the simulation results obtained with the finest grid are presented and discussed. The fine grid consisted of $1152 \times 360 \times 360$ grid points, in the x-, y- and the z- direction, respectively. The grid is uniform in each direction with a grid resolution in wall units of $\Delta x^+ \approx 15$, $\Delta y^+_{max} \approx 5$ and $\Delta z^+_{max} \approx 5$.

Table 1. Hydraulic properties of the semi-filled pipe flow simulation.

	h/D	D	Re_b	U_b	Fr	u_*/U_b
1	52%	0.1004	30010	0.289	0.43	0.054

3. RESULTS

Figure 2 presents profiles of the streamwise time-averaged velocity (a), the streamwise (b), vertical (c) turbulent intensities and turbulent kinetic energy (TKE) (d) in the centre of a semi-filled pipe as predicted by the LES and as measured in the experiment, data of which is published in Ng et al. (2018). In general, the LES results agree very well with the experiments, except a slightly underestimation of the mean velocity near the water surface and a slightly overestimation of the vertical turbulent intensity near the pipe's bottom wall. The so-called 'velocity dip' phenomenon, where the location of the maximum streamwise velocity occurs below the free surface, is well predicted by the LES in partially-filled pipe flow in figure 2(a). The normalized streamwise turbulence intensity and TKE profiles, figs. 2 (b) and (d), peak at $z/h \approx 0.05$, and decrease quickly outside the boundary layer between $0.05 < z/h < 0.1$ and after which it follows a steady linear decrease with depth between $0.1 < z/h < 0.6$. At depth $z/h > 0.6$, and then remain constant until close to the water surface where the values increase suggesting interaction of the flow with the water surface. The vertical turbulence intensity (figure 2c), $\langle w'_{rms} \rangle_x$, peaks a bit further away from the pipe wall than the streamwise component, i.e. at $z/h \approx 0.08$ and, as expected is attaining zero at the water surface because it is a boundary.

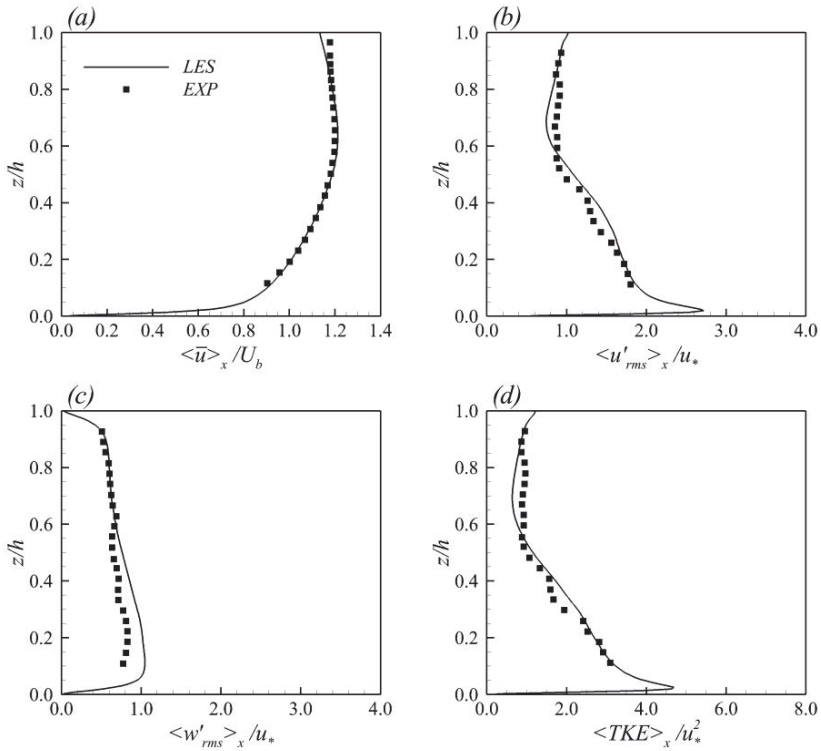

Figure 2. Profiles of the streamwise time-averaged velocity (a), the streamwise (b), vertical (c) turbulent intensities and turbulent kinetic energy (TKE) (d) in the centre of the semi-filled pipe.

Figure 3 plots contours of the time- and streamwise- averaged strength of the secondary flow normalized with the bulk velocity U_s/U_b (a) and streamlines of the secondary flow near the corner between the pipe wall and the water surface (b). The secondary flow strength is calculated as $U_S = \sqrt{\langle\bar{v}\rangle^2+\langle\bar{w}\rangle^2}$. Also plotted are time-averaged secondary flow vectors. First of all, U_s/U_b is largest near the water surface and in the vicinity of the pipe centre line. A pair of symmetric vortices along the pipe centre line is observed, where in the centre of the vortices U_s/U_b is relatively weak. The downward flow from the water surface does not reach to the bottom wall but diverges around $z/R \approx -0.5$ towards the wall. Besides there are small vortices at the corner between the water surface and the pipe walls as shown in figure 3(b). This corner vortex is very small and only $y/R \approx 0.05$ wide.

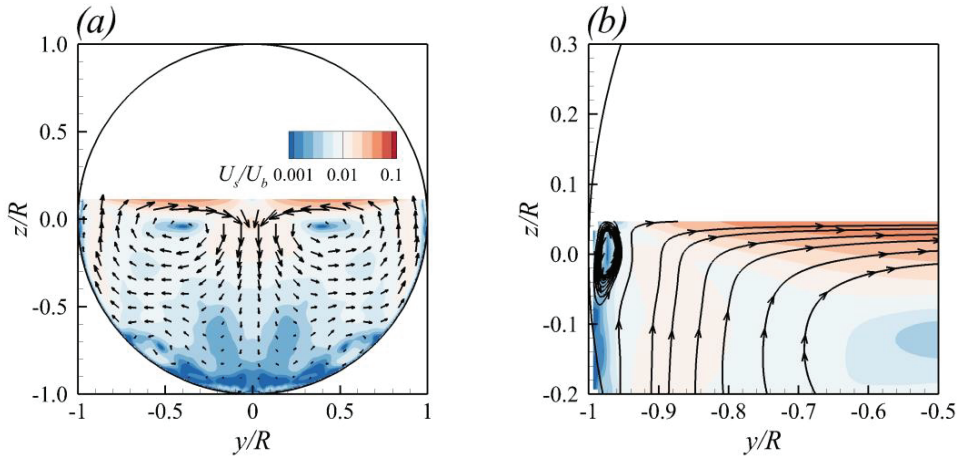

Figure 3. (a) Contours of the time-averaged secondary flow strength normalized with the bulk velocity U_s/U_b, (b) Streamlines of the secondary flow near the corner between the pipe wall and the water surface.

The budget of the turbulent kinetic energy is analyzed in light of the origin of secondary currents in pipe flows. The TKE budget is shown as follows (Nikora and Roy 2012):

$$\underbrace{\frac{\partial k}{\partial t}}_{} + \underbrace{\overline{u_j}\frac{\partial k}{\partial x_j}}_{Convection} = -\frac{1}{\rho}\frac{\partial \overline{u_i' p'}}{\partial x_i} - \underbrace{\frac{1}{2}\frac{\partial \overline{u_j' u_j' u_i'}}{\partial x_i}}_{Transport} + \nu\frac{\partial^2 k}{\partial x_i^2} - \underbrace{\overline{u_i' u_j'}\frac{\partial \overline{u_i}}{\partial x_j}}_{Production} - \underbrace{\nu\frac{\partial u_i'}{\partial x_j}\frac{\partial u_i'}{\partial x_j}}_{Dissipation} \quad [3]$$

The flow is fully developed so that the rate of change of TKE is zero. Pressure diffusion (the first term on the right-hand side (RHS) of equation [3] and molecular viscous transport (the third term on the RHS in equation [3]) are usually negligible compared to the other terms in the equations (Nikora and Roy 2012). Therefore, the four main terms comprising the TKE budget are the TKE convection (TKE_c), TKE production (TKE_p), and TKE turbulent transport (TKE_t), and TKE Dissipation (TKE_d). Figure 4 shows these four components for the semi-filled pipe flow. the highest magnitude of TKE_c occurs only in the two corners of pipe wall and water surface, suggesting that secondary currents origin from these locations. With approaching the water surface along the pipe wall, both the TKE_p and TKE_d decrease dramatically (figures 4b and 4c). While the reduction rate for TKE_p is higher than the TKE_d, which results in a positive TKE_t at the corner of pipe wall and water surface (figure 4d). Due to the absence of shear, TKE production and TKE dissipation are both small near the water surfaces, which has also been reported by Hsu et al. (2000) based on their low aspect ratio open duct flow experiments and simulations.

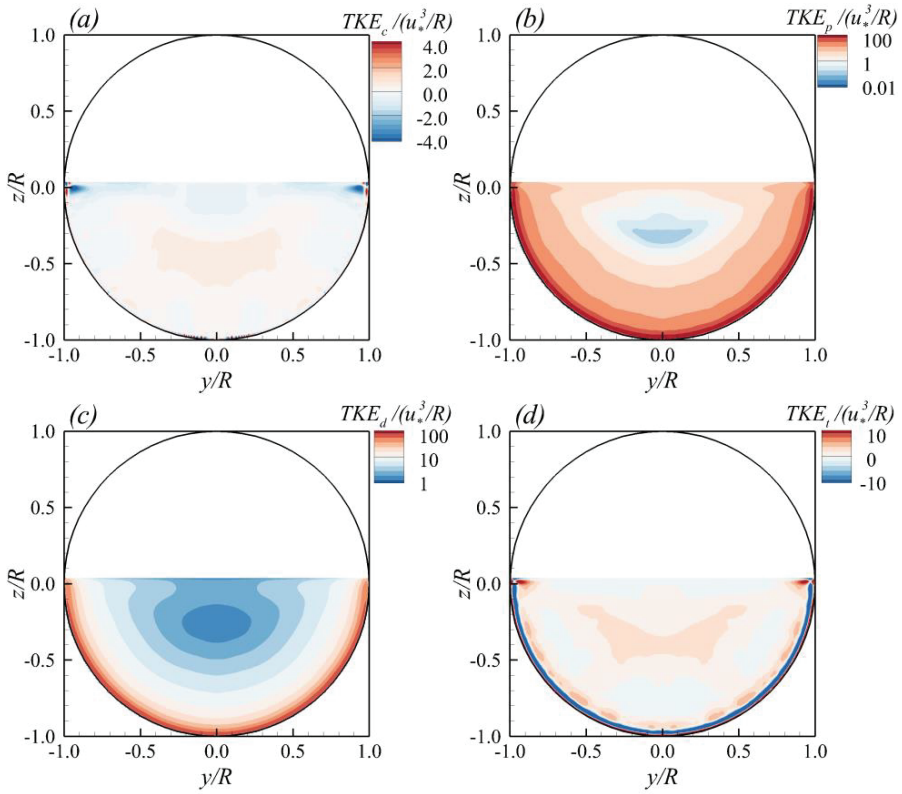

Figure 4. Contours of the TKE convection (a), TKE production (b), TKE dissipation (c), and TKE transport (d) in the semi-filled pipe flow.

Figure 5 presents the iso-surface of Q=300 (b) for the semi-filled pipe flow. There are less numbers of coherent structures near the pipe centreline at y/R=0, where the secondary flow transports high-momentum fluid towards the pipe wall. The absence of coherent structures near the pipe centreline for partially filled flow is also confirmed by Ng et al. (2021), who show that large-scale cells populate the corners where the pipe wall meets the water surface. Moreover, the coherent structures are aligned in the streamwise direction and almost of constant length.

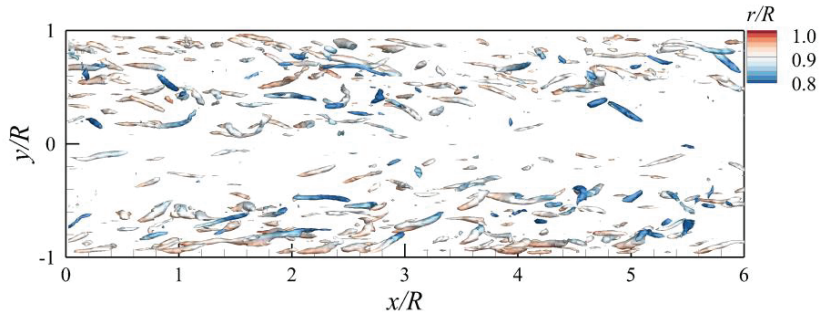

Figure 5. The iso-surface of Q=300 for the semi-filled pipe flow. The Iso-surface is contoured with distance from the pipe center, r/R and the plots are from top view.

Figure 6 presents the normalized instantaneous water surface fluctuation (a) and vertical velocity (b) at the free surface. The dashed lines shown in both figures are at the same locations. There are several locations (marked as dashed lines) where surface boils or dips occur immediately downstream of high and low vertical velocities, respectively. These surface boils or dips originate from the corner of pipe wall and free surface and extend spanwisely with a small angle to the streamwise direction. The locations coincide with that of streamwise aligned coherent structures (figure5). This suggests a direct link between the water surface fluctuations and the coherent structures at the corner of pipe wall and water surface.

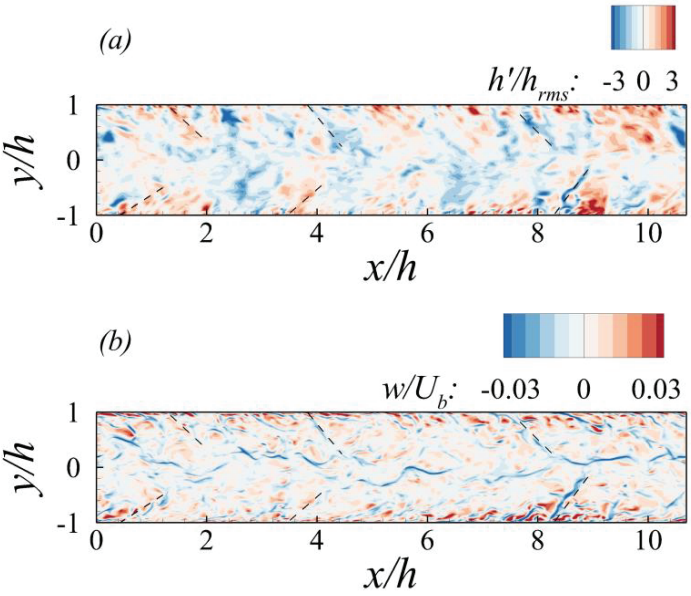

Figure 6. The normalized instantaneous water surface fluctuation (a) and vertical velocity (b) at the free surface.

Figure 7 shows pre-multiplied spectra of h' (a), u' (b), v' (c) and w' (d) along the spanwise direction. The highest pre-multiplied spectra of h' is found very close to the pipe wall at a broad frequency range, i.e. 3<f<10. The magnitude decreases with increasing distance from the wall (Fig. 6a). In Fig. 6(b) the shape of the u' pre-multiplied spectra is very similar to the h' pre-multiplied spectra, i.e. higher when moving towards the pipe walls. However, the peak frequency of u' spectra is in a lower range f<6Hz compared with the h' spectra. In Fig. 6(c), the v' spectra is highest at the pipe centreline where the secondary flow confluent. Finally, a strong peak of the w' pre-multiplied spectra very close to the pipe wall in the range 3Hz<f<11Hz, consistent with the frequency of highest h' spectra is observed. Figure 7 suggests the water surface fluctuation is mainly caused by the vertical velocity fluctuation adjacent to the wall.

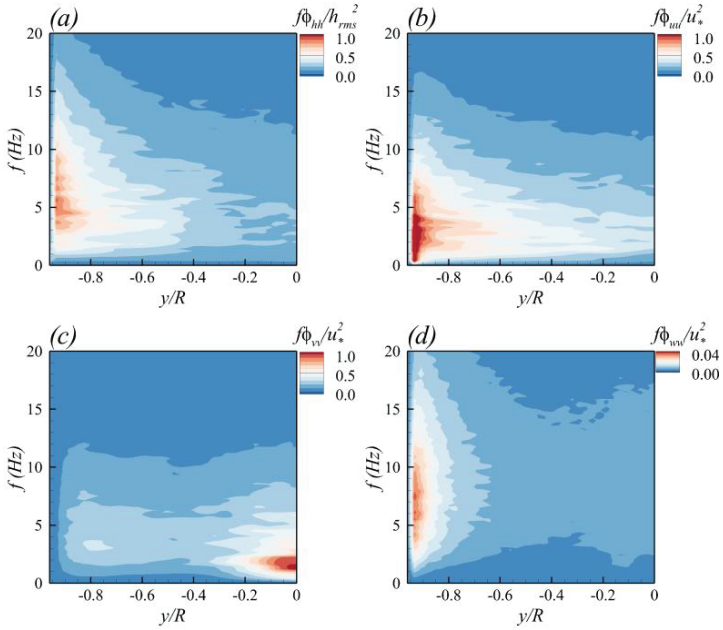

Figure 7. Pre-multiplied spectra of h' (a), u' (b), v' (c) and w' (d) along the spanwise direction.

4. CONCLUSIONS

Large eddy simulation of turbulent flow in a semi-filled pipe was performed. The simulation was validated first and predicted centreline profiles of the time-averaged streamwise velocity, normal stresses and turbulent kinetic energy (TKE) were found to be in very good agreement with recently published experimental data (Ng et al. 2018). The presence of a time-averaged main secondary flow, occupying the whole water depth and a side vortex were observed by examination of the secondary velocity vectors and streamlines. The origin of the mean secondary flow was examined by the TKE budget. It suggests that secondary currents origin from the corner between the water surface and the pipe wall. Production of TKE at this corner is larger than the sum of turbulent transport and dissipation, which results in a mean convection of TKE by secondary flows. The secondary currents convect wall-generated hairpin vortices away from the centreline and towards the water surface. Free surface fluctuations were observed which are closely related to these hairpin vortices. This was confirmed by comparing the pre-multiplied spectra of the free surface and velocity fluctuations.

5. ACKNOWLEDGEMENTS

Financial support for this work is provided by the EPSRC/UK project *Distributed Fibre-optic Cable Sensing for Buried Pipe Infrastructure* **EP/S016376/1**. The authors would like to acknowledge the support of the high-performance cluster centers of the University College London and of Tsinghua University.

6. REFERENCES

Albayrak, I. (2008). *An experimental study of coherent structures, secondary currents and surface boils and their interrelation in open-channel flow* (No. THESIS). EPFL.

Berthelsen, P. A., and Ytrehus, T. (2007). Stratified smooth two-phase flow using the immersed interface method. *Computers and fluids*, *36*(7), 1273-1289.

Birvalski, M., Tummers, M. J., Delfos, R., and Henkes, R. A. W. M. (2014). PIV measurements of waves and turbulence in stratified horizontal two-phase pipe flow. *International journal of multiphase flow*, *62*, 161-173.

Bradshaw, P. (1987). Turbulent secondary flows. *Annual review of fluid mechanics*, *19*(1), 53-74.

Clark, S. P., and Kehler, N. (2011). Turbulent flow characteristics in circular corrugated culverts at mild slopes. *Journal of Hydraulic Research*, *49*(5), 676-684.

Duan, J., Gong, J., Yao, H., Deng, T., and Zhou, J. (2014). Numerical modeling for stratified gas–liquid flow and heat transfer in pipeline. *Applied energy*, *115*, 83-94.

Ead, S. A., Rajaratnam, N., Katopodis, C., and Ade, F. (2000). Turbulent open-channel flow in circular corrugated culverts. *Journal of Hydraulic Engineering*, *126*(10), 750-757.

Enfinger, K. L., and Kimbrough, H. R. (2004). Scattergraph Principles and Practice a Comparison of Various Applications of the Manning Equation. In *Pipeline Engineering and Construction: What's on the Horizon?* (pp. 1-13).
Enfinger, K. L., and Schutzbach, J. S. (2005). Scattergraph Principles and Practice: Camp's Varying Roughness Coefficient Applied to Regressive Methods. In *Pipelines 2005: Optimizing Pipeline Design, Operations, and Maintenance in Today's Economy* (pp. 72-83).
Fang, H. W., Liu, Y., and Stoesser, T. (2017). Influence of boulder concentration on turbulence and sediment transport in open‐channel flow over submerged boulders. *Journal of Geophysical Research: Earth Surface*, *122*(12), 2392-2410.
Fullard, L. A., and Wake, G. C. (2015). An analytical series solution to the steady laminar flow of a Newtonian fluid in a partially filled pipe, including the velocity distribution and the dip phenomenon. *IMA Journal of Applied Mathematics*, *80*(6), 1890-1901.
Hinze, J. O. (1967). Secondary currents in wall turbulence. *The Physics of Fluids*, *10*(9), S122-S125.
Hsu, T. Y., Grega, L. M., Leighton, R. I., and Wei, T. (2000). Turbulent kinetic energy transport in a corner formed by a solid wall and a free surface. *Journal of Fluid Mechanics*, *410*, 343-366.
Kim, K. C., and Adrian, R. J. (1999). Very large-scale motion in the outer layer. *Physics of Fluids*, *11*(2), 417-422.
Knight, D. W., and Sterling, M. (2000). Boundary shear in circular pipes running partially full. *Journal of Hydraulic Engineering*, *126*(4), 263-275.
Liu, Y., Fang, H., Huang, L., and He, G. (2019a). Numerical simulation of the production of three-dimensional sediment dunes. *Physics of Fluids*, *31*(9), 096603.
Liu, Y., Reible, D., Hussain, F., and Fang, H. (2019b). Role of bioroughness, bioirrigation, and turbulence on oxygen dynamics at the sediment‐water interface. *Water Resources Research*, *55*(10), 8061-8075.
Liu, Y., Stoesser, T., Fang, H., Papanicolaou, A., and Tsakiris, A. G. (2017). Turbulent flow over an array of boulders placed on a rough, permeable bed. *Computers and Fluids*, *158*, 120-132.
McSherry, R., Chua, K., Stoesser, T., and Mulahasan, S. (2018). Free surface flow over square bars at intermediate relative submergence. *Journal of Hydraulic Research*, *56*(6), 825-843.
Nezu, I. (2005). Open-channel flow turbulence and its research prospect in the 21st century. *Journal of Hydraulic Engineering*, *131*(4), 229-246.
Ng, H. C. H., Collignon, E., Poole, R. J., and Dennis, D. J. (2021). Energetic motions in turbulent partially filled pipe flow. *Physics of Fluids*, *33*(2), 025101.
Ng, H. C. H., Cregan, H. L., Dodds, J. M., Poole, R. J., and Dennis, D. J. (2018). Partially filled pipes: experiments in laminar and turbulent flow. *Journal of Fluid Mechanics*, *848*, 467-507.
Nicoud, F., and Ducros, F. (1999). Subgrid-scale stress modelling based on the square of the velocity gradient tensor. *Flow, turbulence and Combustion*, *62*(3), 183-200.
Nikora, V., and Roy, A. G. (2012). Secondary flows in rivers: Theoretical framework, recent advances, and current challenges. *Gravel bed rivers: Processes, tools, environments*, 3-22.
Osher, S., and Sethian, J. A. (1988). Fronts propagating with curvature-dependent speed: Algorithms based on Hamilton-Jacobi formulations. *Journal of computational physics*, *79*(1), 12-49.
Pinelli, A., Uhlmann, M., Sekimoto, A., and Kawahara, G. (2010). Reynolds number dependence of mean flow structure in square duct turbulence. *Journal of fluid mechanics*, *644*, 107-122.
Pirozzoli, S., Modesti, D., Orlandi, P., and Grasso, F. (2018). Turbulence and secondary motions in square duct flow. *Journal of Fluid Mechanics*, *840*, 631-655.
Prandtl, L. (1926). Uber die ausgebildete Turbulenz, in “Verhandl. II,” Intern. In *Kongress Techn. Mech., Zürich* (pp. 62-75).
Swaffield, J. A., and Bridge, S. (1983). Applicability of the Colebrook-White formula to represent frictional losses in partially filled unsteady pipeflow. *JOURNAL OF RESEARCH of the National Bureau of Standards*, *88*(6), 389.
Uhlmann, M. (2005). An immersed boundary method with direct forcing for the simulation of particulate flows. *Journal of Computational Physics*, *209*(2), 448-476.
Uhlmann, M., Pinelli, A., Kawahara, G., and Sekimoto, A. (2007). Marginally turbulent flow in a square duct. *Journal of fluid mechanics*, *588*, 153-162.
Vollestad, P., Angheluta, L., and Jensen, A. (2020). Experimental study of secondary flows above rough and flat interfaces in horizontal gas-liquid pipe flow. *International Journal of Multiphase Flow*, *125*, 103235.

